Science of the Total Environment 772 (2021) 145607

Contents lists available at ScienceDirect

Science of the Total Environment

journal homepage: www.elsevier.com/locate/scitotenv

Long-term trends of surface and canopy layer urban heat island intensity in 272 cities in the mainland of China

Rui Yao [a,b], Lunche Wang [a,b,*], Xin Huang [c,d], Yuting Liu [a,b], Zigeng Niu [a,b], Shaoqiang Wang [a,b], Lizhe Wang [e,f]

[a] Key Laboratory of Regional Ecology and Environmental Change, School of Geography and Information Engineering, China University of Geosciences, Wuhan 430074, China
[b] Hunan Key Laboratory of Remote Sensing of Ecological Environment in Dongting Lake Area, School of Geography and Information Engineering, China University of Geosciences, Wuhan 430074, China
[c] School of Remote Sensing and Information Engineering, Wuhan University, Wuhan 430079, China
[d] State Key Laboratory of Information Engineering in Surveying, Mapping and Remote Sensing, Wuhan University, Wuhan 430079, China
[e] School of Computer Science, China University of Geosciences, Wuhan 430074, China
[f] Hubei Key Laboratory of Intelligent Geo-Information Processing, China University of Geosciences, Wuhan 430074, China

HIGHLIGHTS

- Temporal trends of CLUHII and SUHII were investigated in 272 cities in mainland China.
- CLUHII and SUHII increased significantly in over half of the cities in spring and summer.
- Human activities were the major driving forces for the increase in CLUHII and SUHII.

GRAPHICAL ABSTRACT

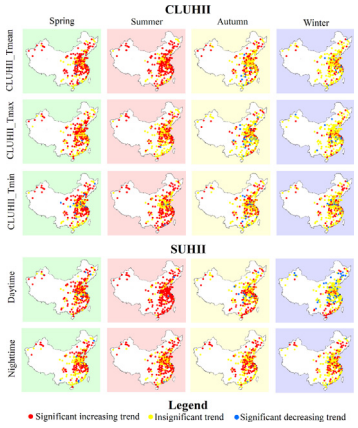

ARTICLE INFO

Article history:
Received 26 November 2020
Received in revised form 29 January 2021
Accepted 29 January 2021
Available online 4 February 2021

Editor: Scott Sheridan

Keywords:
Urban heat island
Urbanization
Remote sensing
Air temperature
Land surface temperature
The mainland of China

ABSTRACT

The canopy layer urban heat island (CLUHI) and surface urban heat island (SUHI) refer to higher canopy layer and land surface temperatures in urban areas than in rural areas, respectively. The long-term trends of CLUHIs are poorly understood at the regional scale. In this study, 1 km resolution air temperature (Ta) data for the 2001–2018 period in the mainland of China were mapped using satellite data and station-based Ta data. Subsequently, the temporal trends of the CLUHI and SUHI intensities (CLUHII and SUHII, respectively) were investigated in 272 cities in the mainland of China. The Ta was estimated with high accuracy, with a root mean square error ranging from 0.370 °C to 0.592 °C. The CLUHII and SUHII increased significantly in over half of the cities in spring and summer, over one-third of the cities in autumn, and over one-fifth of the cities in winter. The trends of the nighttime SUHII were strongly related to the CLUHII calculated using mean and minimum Ta (correlation coefficients ranging from 0.613 to 0.770), whereas the relationships between the trends of the daytime SUHII and CLUHII were relatively weak. Human activities were the major driving forces for the increase in the CLUHII and SUHII. The difference in impervious surfaces between urban and rural areas was significantly correlated with the CLUHII and SUHII in approximately half of the cities. Meteorological factors were significantly

* Corresponding author at: School of Geography and Information Engineering, China University of Geosciences, Wuhan 430074, China.
E-mail address: wang@cug.edu.cn (L. Wang).

https://doi.org/10.1016/j.scitotenv.2021.145607

correlated with the CLUHII and SUHII in few cities. This study highlights the trends of the significant increase in the CLUHII and SUHII in the mainland of China, which may have negative effects on humans and the environment.

1. Introduction

Rapid urbanization has strongly modified the Earth's surface in the past several decades. It can lead to higher subsurface, surface, and air temperatures (Ta) in urban areas compared with those in surrounding rural areas. This phenomenon is called the urban heat island (UHI) effect, which can affect human comfort and health (Patz et al., 2005), increase energy consumption (Santamouris et al., 2001; Akbari et al., 2015), and alter water and air quality (Lai and Cheng, 2009; Grimm et al., 2008). To support the design of adaptive strategies, a comprehensive understanding of the UHI effect is needed.

The UHI can generally be grouped into three types, namely subsurface UHI (SubUHI) (Zhan et al., 2014), surface UHI (SUHI) (Zhou et al., 2019), and canopy layer UHI (CLUHI) (Pichierri et al., 2012). The SubUHI, SUHI, and CLUHI refer to higher subsurface, surface, and canopy layer temperatures in urban areas compared with those in nearby rural areas, respectively. The SubUHI can be monitored by observation stations and modeled by satellite remote sensing. Analysis of the SubUHI effect is challenging, and has only been conducted in few studies (Zhan et al., 2014). The SUHI effect is commonly monitored by satellite remote sensing, which provides spatially continuous land surface temperature (Ts) data. The spatiotemporal variations in the SUHI effect have been widely studied (Du et al., 2016; Peng et al., 2018; Peng et al., 2012; Yao et al., 2019; Zhou et al., 2014). For example, Yao et al. (2019) investigated the trends of the SUHI intensity (SUHII) in 397 global cities from 2001 to 2017. Trends of significant increases in annual daytime and nighttime SUHII were found in 42.1% and 30.5% of cities, respectively. Increased rural vegetation coverage is an important driver for the increase in the daytime SUHII (Yao et al., 2019). The CLUHI effect is normally studied using Ta data from meteorological stations at 2 m above the ground (Hu et al., 2019; Voogt and Oke, 2003). Ta data from meteorological stations have a high temporal resolution and accuracy, but are spatially discontinuous. Some advanced methods have also been used to analyze the CLUHI effect. Some studies used numerical models (Li et al., 2019; McCarthy et al., 2010; Oleson et al., 2010). For instance, Li et al. (2019) first created a 1 km resolution Ta map using the Weather Research and Forecasting Model, and then analyzed the CLUHI intensity (CLUHII) in Berlin, Germany. The results showed that the nighttime CLUHII was prominent (1.62 °C) but the daytime CLUHII was insignificant (−0.04 °C). Some studies first mapped Ta data using satellite variables and observed Ta data, and then analyzed the CLUHI effect (Li and Zha, 2019b; Liu et al., 2020). For example, Li and Zha (2019b) first developed a 1 km resolution Ta dataset, and then analyzed the CLUHII in 32 cities in China. The results showed that the annual daytime and nighttime CLUHIIs ranged from 0.2 °C to 2.2 °C and from 0.3 °C to 2.4 °C, respectively. These methods are promising because they can retain the advantages of meteorological station monitoring (e.g., high temporal resolution) and make up for its shortcomings (e.g., spatial discontinuity).

With respect to human health impacts, the CLUHI effect may be more important than the SUHI effect because human skin is directly in contact with the atmosphere rather than the land surface (Anniballe et al., 2014; Zhou et al., 2016). The spatiotemporal variations in the CLUHI effect and their associated determinants have been widely investigated (Arnfield, 2003; Li et al., 2019; Li and Zha, 2019b; Liu et al., 2020; Oke, 1981; Pichierri et al., 2012). However, there are still some gaps in the current research on the CLUHI effect. For example, the long-term trends of the CLUHI effect and its associated drivers are still poorly understood at the regional scale. By using the observed Ta data from meteorological stations, some studies found that the CLUHI effect has intensified significantly in the past few decades (Liao et al., 2017b; Ren and Zhou, 2014; Ren et al., 2008; Yang et al., 2011; Varquez and Kanda, 2018; Park et al., 2017; Founda et al., 2015). However, most of these studies only analyzed the regional averaged CLUHI effect and did not reveal the drivers of the trends of the CLUHI effect. In addition, these studies have some uncertainties because the meteorological stations are sparsely distributed. Climate models have also been used to analyze the changes of CLUHI. For example, McCarthy et al. (2010) projected the changes of CLUHI with future climate change using an urban scheme within a global climate model by 2050. The results showed that future warming can reduce the CLUHII by 6% at the global scale. However, climate models may have uncertainty and the result may be largely affected by model parameters (Hourdin et al., 2017; McCarthy et al., 2010). Liu et al. (2020) analyzed the CLUHI effect in southern China using spatially continuous Ta data modeled by satellite data. The results showed that the average CLUHII was 1.490 °C and the average trend of the CLUHI was 0.011 °C/year. However, Liu et al. (2020) only analyzed the CLUHI effect for 33 cities in 3 provinces in China. In addition, the time series used by Liu et al. (2020) was only 13 years (2003–2015). Therefore, the present study aimed to conduct comprehensive analyses of the temporal trends of the CLUHI effect and their drivers. The SUHI effect was also analyzed and compared with the CLUHI effect. The Ta data used in this study were mapped using satellite variables and a matching learning algorithm. The remaining manuscript is organized as follows. Section 2 presents the study area and data. Section 3 presents the methods used in this study, including the Ta estimation and validation, methods for analyzing the trends of the CLUHI effect and SUHI effect, and drivers of the trends of the CLUHI effect and SUHI effect. Section 4 presents the main results, including the accuracy of the estimated Ta, temporal trends of the CLUHI effect and SUHI effect, and their drivers. Section 5 discusses the methods and results of this study. A summary is presented in Section 6.

2. Study areas and data

2.1. Study areas

China is the most populous developing country in the world. In addition, the mainland of China has experienced unprecedented rapid urbanization since the reform and opening-up. The urban population increased from 192 million in 1980 to 775 million in 2015 (United Nations, 2018). This makes it crucial to reveal the temporal trends of the UHI effect in the mainland of China. In this work, a total of 272 cities with urban areas larger than 50 km^2 in the mainland of China were selected as the study areas (Fig. 1). These cities are mainly distributed in eastern China. The elevations of these 272 cities range from 3 m (Yangzhou) to 2285 m (Xining). The climate differs greatly across these cities, with an annual mean Ta ranging from 2.5 °C (Yichun) to 24.6 °C (Haikou) and an annual total precipitation ranging from 65 mm (Korla) to 2874 mm (Yangjiang).

2.2. Data and preprocessing

The data used in the present study and their associated information are presented in Table 1. First, Ta (including mean, maximum, and minimum Ta), precipitation, wind speed, and sunshine duration data from 697 meteorological stations for the 2001–2018 period were derived from the China Meteorological Data Service Center. The spatial

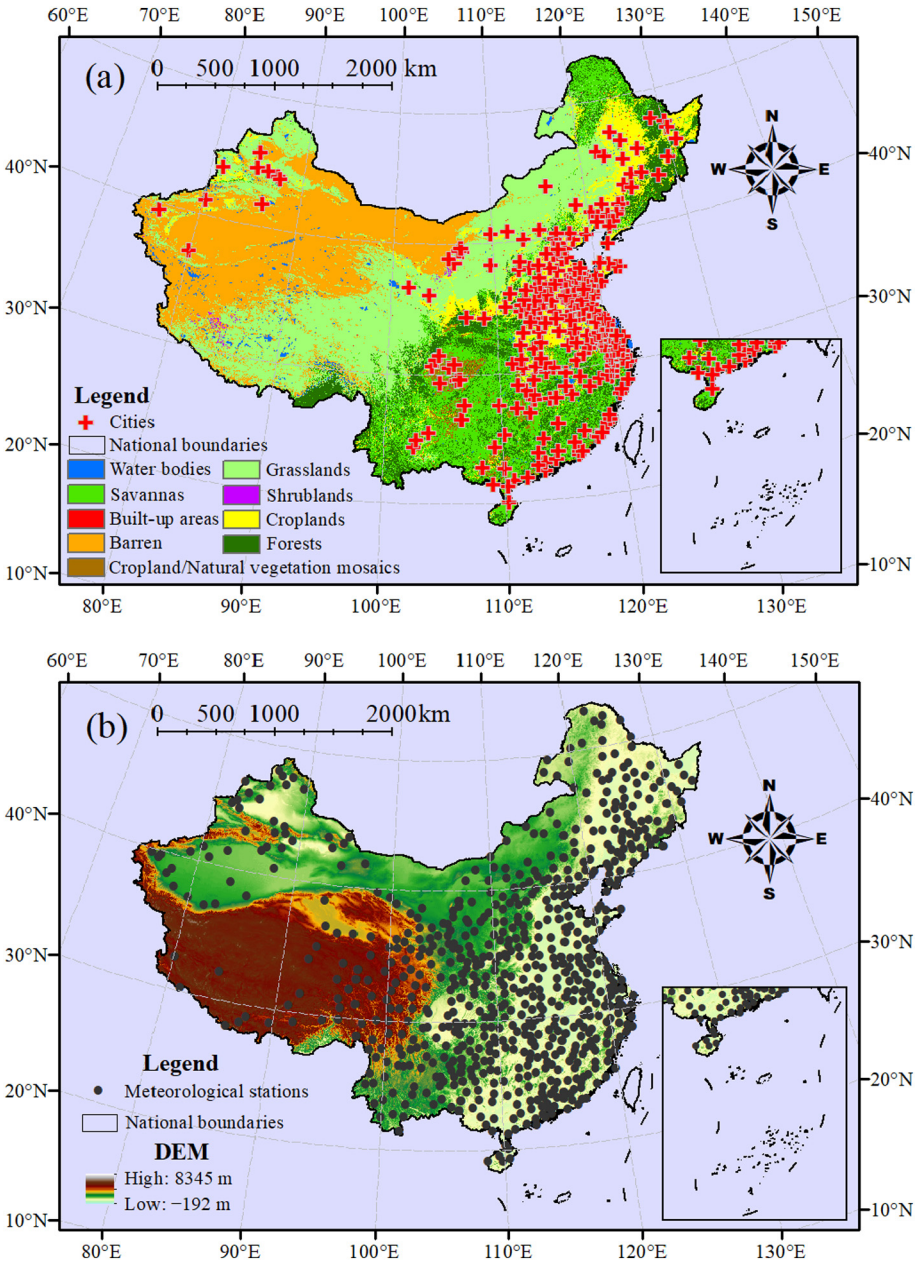

Fig. 1. (a) Spatial distribution of the 272 selected cities. The background map is the MODIS MCD12Q1 land cover data in 2018. (b) Spatial distribution of the 697 meteorological stations. The background map is the elevation data.

distribution of the meteorological stations is shown in Fig. 1b. Second, MODIS MOD11A2 Ts (including daytime Ts, nighttime Ts, clear-sky days, and clear-sky nights), MOD13A3 enhanced vegetation index (EVI), and MCD12Q1 land cover type data were derived from the NASA Level-1 and Atmosphere Archive & Distribution System. Third, clear-sky solar radiation, slope, aspect, latitude, and longitude data were calculated using ArcGIS software. Fourth, elevation (Danielson and Gesch, 2011), topographic index (Marthews et al., 2015), nighttime light (NL) (Li et al., 2020), and impervious surface (IS) (Gong et al., 2020) data were used.

The 500 m resolution land cover data were resampled to 1 km. The proportion of IS (PIS) data with 1 km resolution was calculated from the original 30 m resolution data. The Ta, precipitation, wind speed, sunshine duration, Ts, and EVI data were averaged into one season (spring: March to May; summer: June to August; autumn: September to November; winter: December to February). In the process of averaging, only valid values were used (Yao et al., 2017b; Li et al., 2017). The land cover type, NL, and PIS data were assumed to be the same for the entire year. The topographic index, elevation, slope, aspect, latitude, and longitude data were assumed to be the same for the 2001–2018 period.

The land cover type (according to MODIS land cover data) of 6, 157, 129, 12 and 293 out of 697 meteorological stations are water bodies, natural vegetation, croplands, barelands and urban areas, respectively. The PIS in 2 km buffer areas around 302, 157, 132, 74 and 32 out of 697 meteorological stations are within the range of 0–20%, 20–40%, 40–60%, 60–80% and 80–100%, respectively.

3. Methods

3.1. Ta estimation

Accurate estimation of Ta is the basis of the CLUHI effect study. Therefore, this study chose as many variables as possible to estimate the Ta. A total of 16 variables were used, namely daytime Ts, nighttime

Table 1
Data used in this study and their associated information. Ta: air temperature. Ts: land surface temperature. EVI: enhanced vegetation index. NL: nighttime light. IS: impervious surface.

Data	Spatial resolution	Temporal resolution	Source	Time period
Mean Ta	Point	1 day	http://data.cma.cn/	2001–2018
Maximum Ta	Point	1 day	http://data.cma.cn/	2001–2018
Minimum Ta	Point	1 day	http://data.cma.cn/	2001–2018
Precipitation	Point	1 day	http://data.cma.cn/	2001–2018
Wind speed	Point	1 day	http://data.cma.cn/	2001–2018
Sunshine duration	Point	1 day	http://data.cma.cn/	2001–2018
Daytime Ts	1 km	8 days	https://ladsweb.modaps.eosdis.nasa.gov/search/	2001–2018
Nighttime Ts	1 km	8 days	https://ladsweb.modaps.eosdis.nasa.gov/search/	2001–2018
Clear sky days	1 km	8 days	https://ladsweb.modaps.eosdis.nasa.gov/search/	2001–2018
Clear sky nights	1 km	8 days	https://ladsweb.modaps.eosdis.nasa.gov/search/	2001–2018
EVI	1 km	1 month	https://ladsweb.modaps.eosdis.nasa.gov/search/	2001–2018
Land cover type	500 m	1 year	https://ladsweb.modaps.eosdis.nasa.gov/search/	2001–2018
Topographic index	1 km	No	https://eidc.ac.uk	No
Elevation	1 km	No	Stored in ENVI software	No
Solar radiation	1 km	3 months	Calculated using ArcGIS software	2001–2018
Slope	1 km	No	Calculated using ArcGIS software	No
Aspect	1 km	No	Calculated using ArcGIS software	No
Latitude	1 km	No	Calculated using ArcGIS software	No
Longitude	1 km	No	Calculated using ArcGIS software	No
NL	1 km	1 year	https://doi.org/10.6084/m9.figshare.9828827.v2	2001–2018
IS	30 m	1 year	http://data.ess.tsinghua.edu.cn/	2001–2018

Ts, clear-sky days, clear-sky nights, EVI, elevation, topographic index, solar radiation, aspect, slope, PIS, NL, land cover type, latitude, longitude, and year. The values of the pixels corresponding to meteorological stations were extracted from the following data: daytime Ts, nighttime Ts, clear-sky days, clear-sky nights, EVI, elevation, topographic index, solar radiation, aspect, slope, PIS, NL, and land cover type. In addition, latitude, longitude, and year information corresponding to the Ta from the meteorological station data were directly used.

In this study, Cubist matching learning algorithm (Quinlan, 1992) (detailed information see Appendix) was used to estimate the Ta because it has high accuracy (Zhang et al., 2016; Noi et al., 2017; Xu et al., 2018). The Ta and 16 prediction variables were input into the Cubist model, and the relationship between the Ta and prediction variables was fit. After, the 1 km resolution Ta data were mapped using the fitted relationship and 1 km resolution prediction variable data. The Ta data for the four seasons were estimated separately (but for all years together) because the correlations between the Ta and prediction variables varied by season (Yao et al., 2020).

3.2. Variable selection

The number of prediction variables in this study was large. Some prediction variables may not have a positive effect on the estimation of Ta and may cause an overfitting phenomenon. Therefore, a variable selection method was used (Meyer et al., 2016; Xu et al., 2018). First, all the possible combinations of two variables were input into the Cubist model and the combination with the highest accuracy was used. Second, the remaining variables were separately added to the current combination, and the variable that best improved the accuracy was maintained. Third, the second step was repeated until the accuracy of the Ta estimation could not be improved. By using this variable selection method, 12 variables (daytime Ts, nighttime Ts, clear-sky days, clear-sky nights, elevation, topographic index, solar radiation, aspect, slope, latitude, longitude, and year) were used. Additionally, 4 variables (EVI, PIS, NL and land cover type) had no positive effect on Ta estimation. This is similar to Li and Zha (2019a) and Janatian et al. (2017), which found that vegetation index and variables related to land cover had negligible effect on Ta estimation. The reason for this is that these variables (EVI, PIS, NL and land cover type) significantly correlated with other variables (e.g., Ts) and did not provide additional information when estimating Ta.

3.3. Accuracy validation of Ta estimation

The accuracy of the estimated Ta was first validated. In addition, as the goals of this study were to analyze the trend of the CLUHI effect and its drivers, the accuracies of the interannual variations and trends of Ta were also verified. Meteorological stations that were relocated (360 out of 697 stations) during 2001–2018 were not utilized to validate the accuracies of the interannual variations and trends of the predicted Ta because station relocation can affect the observed interannual variations and trends of Ta. Therefore, the accuracy of the estimated Ta was validated using a modified 10-fold validation method (Yao et al., 2020), which included the following four steps:

(1) Samples from meteorological stations that had not been relocated (337 out of 697) were randomly partitioned into 10 subsets.
(2) Nine subsets partitioned in the previous step and samples from the meteorological stations that were relocated were input into the Cubist model, and the remaining subset was employed to validate the accuracy.
(3) Step (2) was repeated 10 times. For each time, an unused subset was used to validate.
(4) The mean absolute error (MAE), root mean square error (RMSE) and coefficient of determination (R^2) were computed to describe the accuracy of the estimated Ta. The interannual MAE, RMSE and R^2 were computed for each station that was not relocated. The MAE, RMSE and R^2 were calculated to describe the accuracy of the trends (calculated using the linear regression method) of the estimated Ta across 337 stations that were not relocated.

3.4. Analyzing the trends of CLUHI and SUHI

Pixels with a PIS higher than 50% (Mertes et al., 2015; Yao et al., 2018a; Zhou et al., 2014) were considered urban pixels in this study. Cities with urban areas larger than 50 km^2 in 2018 were selected as study areas. Subsequently, a 20 km buffer based on the urban area was generated for each city. In the 20 km buffer, areas with a PIS higher than 0% were excluded, and the remaining areas were considered rural areas. It should be noted that the urban and rural areas in 2018 were used to analyze the UHI effect for the 2001–2018 period, because this strategy can uncover the overall trend of UHI effect, including the trends in newly developed and old urban areas (Yao et al., 2018b, 2019). Finally,

the UHI intensity (UHII, hereafter CLUHII and SUHII) was used to quantify the UHI effect (Peng et al., 2012; Zhou et al., 2014), as follows:

$$\Delta T_1(\mathrm{CLUHII}) = Ta_{urban} - Ta_{rural} \quad (1)$$

$$\Delta T_2(\mathrm{SUHII}) = Ts_{urban} - Ts_{rural} \quad (2)$$

where ΔT_1 and ΔT_2 refer to the CLUHII and SUHII, respectively. Ta_{urban} and Ts_{urban} represent the spatial average urban Ta and Ts, respectively. Ta_{rural} and Ts_{rural} refer to the spatial average rural Ta and Ts, respectively. The CLUHII calculated using the mean, maximum, and minimum Ta was called the CLUHII_Tmean, CLUHII_Tmax, and CLUHII_Tmin, respectively. The SUHII calculated using the daytime and nighttime Ts was called the daytime SUHII and nighttime SUHII, respectively. The temporal trends of the CLUHII and SUHII during 2001–2018 were calculated using a linear regression method.

3.5. Investigating the drivers of the trends of the CLUHI and SUHI effects

ΔEVI, ΔNL, and ΔPIS were calculated using the same method as that in Eqs. (1) and (2). The relationships between the UHII and ΔEVI, ΔNL, ΔPIS, precipitation, wind speed, and sunshine duration were then explored. Pearson's correlation analysis between the UHII and associated determinants was conducted in each city separately across 2001–2018. Pearson's correlation analysis has been widely used to analyze the drivers of the UHI effect in previous studies (Du et al., 2016; Yao et al., 2018b; Zhou et al., 2014). Hierarchical partitioning (HP) analysis was utilized to calculate the relative importance of each factor to the UHI effect (Mac, 2000; Peng et al., 2018). HP analysis can avoid the multicollinearity phenomenon in environmental variables.

4. Results

4.1. Accuracy of Ta estimation

The Cubist model produced accurate Ta estimates (Fig. 2). The MAE, RMSE, and R^2 of the Ta estimation ranged from 0.289 °C to 0.455 °C, 0.370 °C to 0.592 °C, and 0.989 to 0.997, respectively. Seasonally, the MAE and RMSE values in summer were lower than those in other seasons. However, the R^2 in summer was also lower than that in other seasons. This was primarily because the range of the Ta in the mainland of China in summer is significantly lower than that in other seasons (Li and Zha, 2019a; Yao et al., 2020). Diurnally, the accuracy of the maximum Ta was generally lower than the mean and minimum Ta. This can be explained by the weaker correlation between the Ts and maximum Ta than that between the Ts and mean or minimum Ta, which was demonstrated by many previous studies (Kloog et al., 2014; Vancutsem et al., 2010; Dousset, 1989). Furthermore, the MAE, RMSE, and R^2 of the interannual variations in the estimated Ta ranged from 0.289 °C to 0.455 °C, 0.358 °C to 0.568 °C, and 0.547 to 0.827, respectively. The MAE, RMSE,

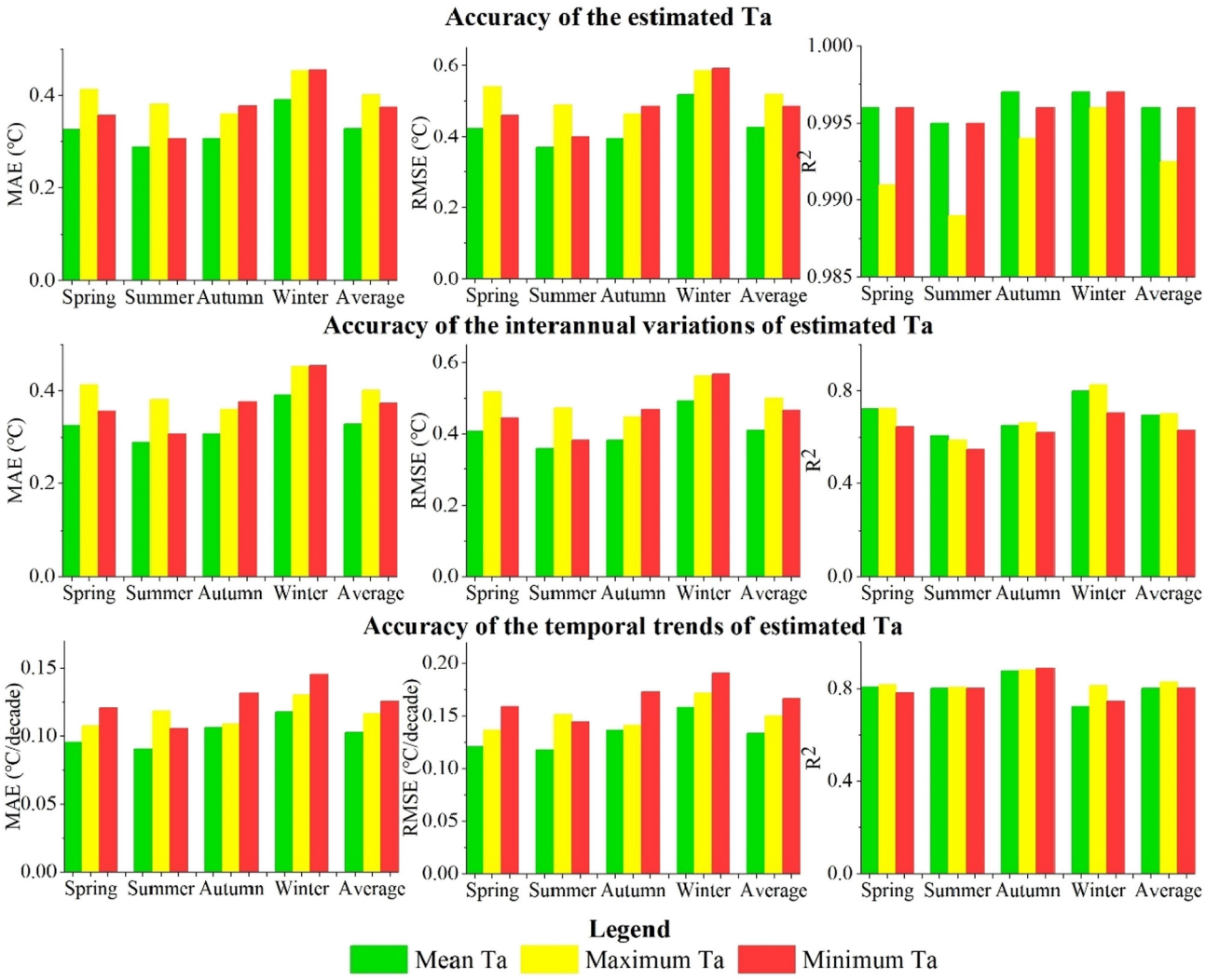

Fig. 2. Accuracy of the estimated air temperature (Ta). MAE: mean absolute error. RMSE: root mean square error. R^2: coefficient of determination.

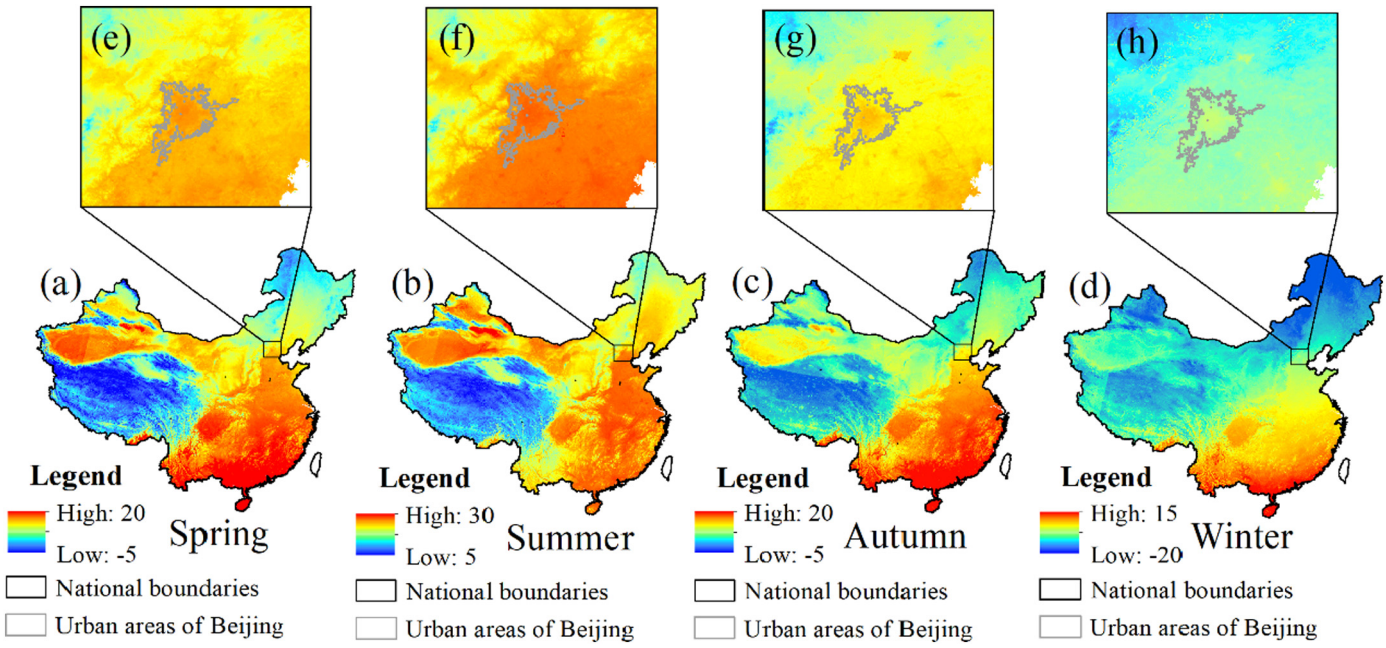

Fig. 3. Spatial distributions of the seasonal mean air temperature (Ta) in the mainland of China in 2018 in (a) spring; (b) summer; (c) autumn; and (d) winter. Spatial distributions of the seasonal mean Ta in Beijing in 2018 in (e) spring; (f) summer; (g) autumn; and (h) winter. Unit: °C.

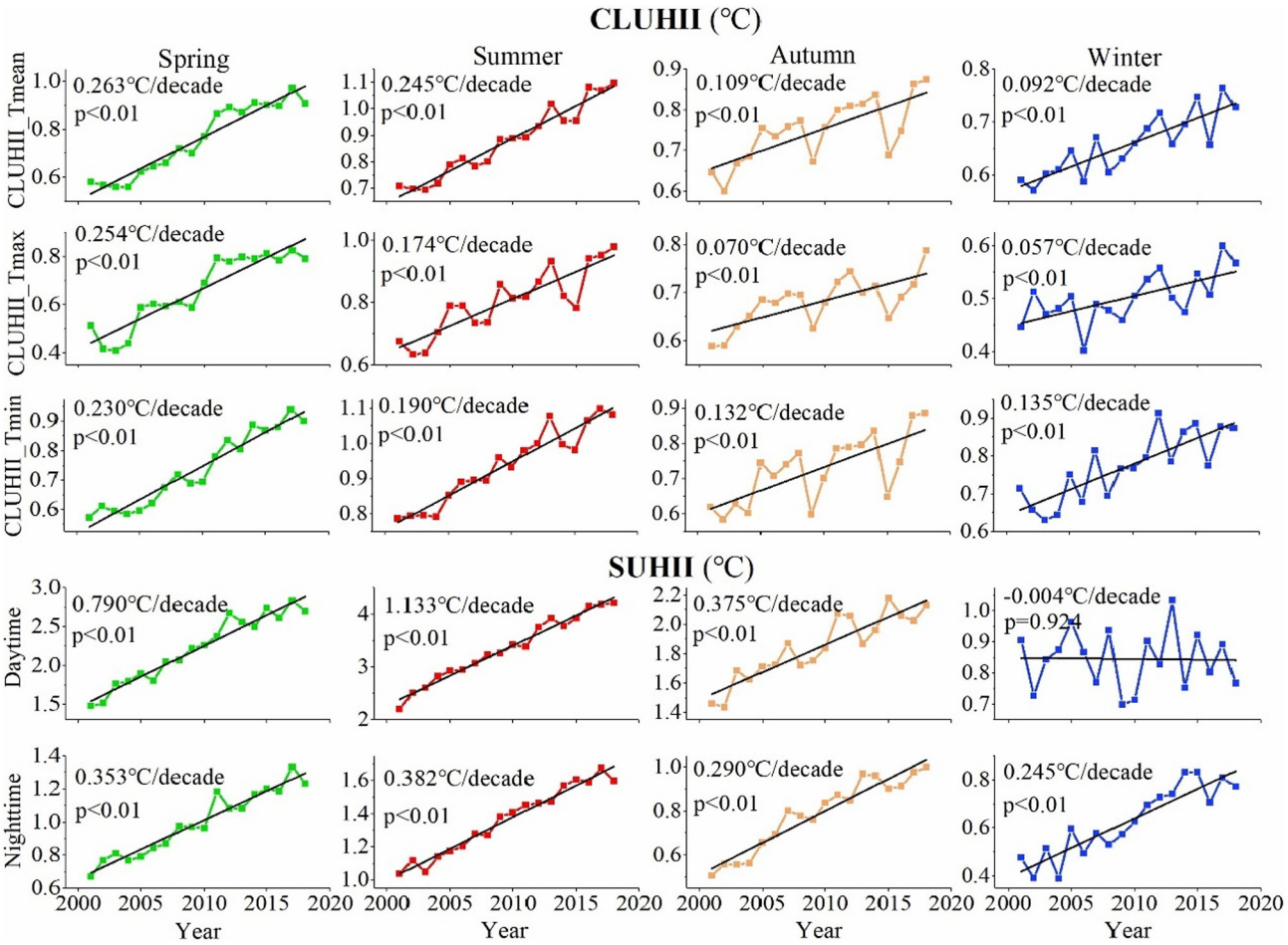

Fig. 4. Trends of the CLUHII and SUHII averaged for 272 cities for the 2001–2018 period.

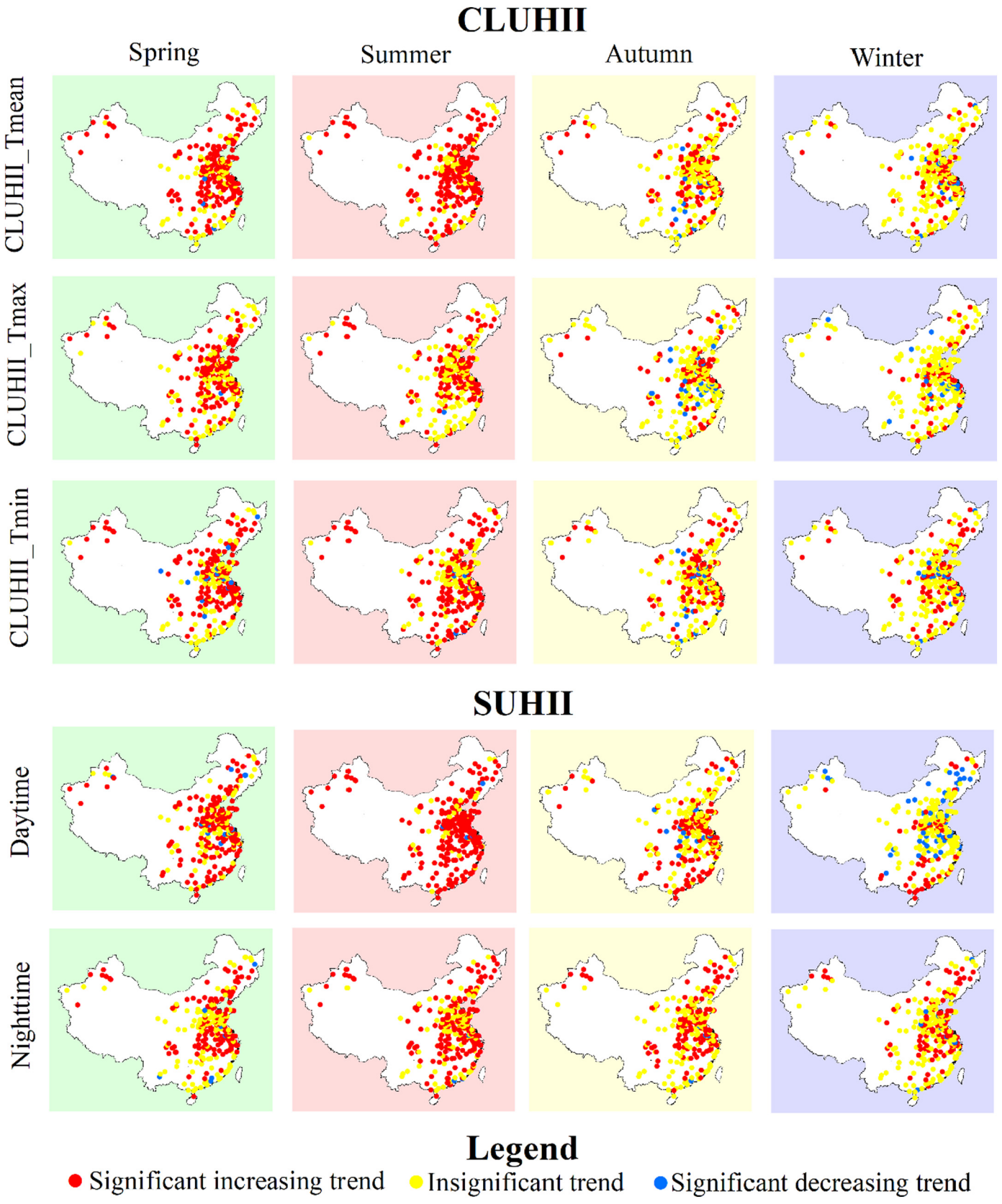

Fig. 5. Spatial distributions of the trends of the CLUHII and SUHII for the 2001–2018 period.

and R^2 of the trends of the estimated Ta ranged from 0.091 °C/decade to 0.145 °C/decade, 0.118 °C/decade to 0.191 °C/decade, and 0.723 to 0.889, respectively. These results suggested that the estimated Ta was temporally consistent with the observed Ta. The accuracy of the Ta estimation in the present study was greater than that in most previous studies (Hooker et al., 2018; Li et al., 2018; Lu et al., 2018; Shen et al.,

2020; Xu et al., 2018; Yao et al., 2020; Yoo et al., 2018; Zhang et al., 2016; Zhou et al., 2020; Zhu et al., 2017). This occurred because (1) the number of prediction variables in this study was large (a total of 12 prediction variables) and (2) this study estimated seasonal Ta, whereas most previous studies estimated daily or monthly Ta. Overall, the accurate Ta dataset ensured the reliability of the following results.

The spatial distributions of the seasonal mean Ta in 2018 are shown in Fig. 3. The mean Ta was higher in summer and lower in winter. Spatially, north China had a lower mean Ta owing to its higher latitude, whereas the Qinghai-Tibet Plateau had a lower mean Ta because of its high elevation. Furthermore, the developed Ta data could resolve the UHI effect well (Fig. 3e–h), thereby indicating that the Ta data are suitable for investigating the UHI effect.

4.2. Trends of the CLUHII and SUHII in the mainland of China

The CLUHII and SUHII increased significantly in the mainland of China during 2001–2018 (Figs. 4 and 5; Table 2). For the 272 cities combined, the increasing rate of CLUHII ranged from 0.057 °C/decade to 0.263 °C/decade ($p < 0.01$ in all cases) (Fig. 4). The SUHII also increased significantly, except for the daytime SUHII in winter. The number of cities with a trend of significant increases in CLUHII and SUHII ranged from 71 to 218 and from 64 to 245, respectively (Table 2). Trends of significant decreases in CLUHII and SUHII were found in few cities.

Trends of Ts and Ta in urban and rural areas averaged for 272 cities for the 2001–2018 period are shown in Table 3. Although the Ts and Ta increased in rural areas, the trends were not statistically significant in most cases. Comparatively, the increasing trends of Ts and Ta in urban areas were significant in many cases, especially in summer. These results suggested that the UHI effect has significantly altered the urban thermal environment since the beginning of the 21st century.

Seasonally, the increasing rates of CLUHII and SUHII in spring and summer were much higher than those in autumn and winter. The number of cities with significantly increasing rates of CLUHII and SUHII in spring and summer was also much greater than that in autumn and winter. These phenomena could be attributed to two main reasons. First, it can be attributed to more significant decreasing trends of ΔEVI in spring and summer than in autumn and winter (more information can be found in the next section). Second, the definition of the season was another reason. Spring, summer, autumn and winter were defined as from March to May, June to August, September to November and December to February, respectively, in this study. This definition will put the majority of dates past the spring equinox (longer day length than night length) in spring and the majority of dates past the autumn equinox (shorter day length than night length) in autumn. Therefore, the increased IS due to urbanization will absorb more solar radiation and lead to higher increasing rates of UHII in spring and summer than in autumn and winter.

Diurnally, the increasing rates of the CLUHII_Tmax were generally lower than those of the CLUHII_Tmean and CLUHII_Tmin. This result echoes those of previous studies (Arnfield, 2003; Liao et al., 2017b; Pichierri et al., 2012). CLUHII_Tmax is generally lower than CLUHII_Tmean or CLUHII_Tmin due to the solar shading effect and advective fluxes during the daytime. It suggested that the differences in maximum Ta between urban and rural areas are generally lower than the differences in mean and minimum Ta between urban and rural areas. The transformation from rural to urban areas will therefore lead to lower increasing rate of CLUHII_Tmax than those of the CLUHII_Tmean and CLUHII_Tmin. In addition, the increasing rate of daytime SUHII was higher than that of nighttime SUHII, except for in winter. This was similar to the results of previous studies (Yang et al., 2019; Yao et al., 2017a), and primarily occurred because the daytime SUHII is more affected by the decreased vegetation cover than nighttime SUHII. Spatially, there was no clear difference in the trends of the UHII, thereby indicating that the trends of increasing UHII were widespread. Finally, the increasing rates of the SUHII were much higher than those of the CLUHII, except for in winter. This can be explained because Ts is more sensitive to changes in land cover and surface characteristics than Ta.

The relationships between the trends of the CLUHII and SUHII are shown in Fig. 6. The trends of the CLUHII were significantly ($p < 0.05$) correlated with those of SUHII in most cases. However, the correlations between the trends of the daytime SUHII and CLUHII were weak, with a correlation coefficient (r) ranging from −0.318 to 0.445. The trends of the nighttime SUHII were strongly related to those of the CLUHII_Tmean (r ranging from 0.613 to 0.738) and the CLUHII_Tmin (r ranging from 0.655 to 0.770). This was primarily because the daytime SUHII is more strongly affected by solar radiation and land cover type than the other types of UHII (Xu et al., 2018). In addition, the correlations between the trends of the daytime SUHII and the CLUHII_Tmax were stronger than those between the daytime SUHII and the CLUHII_Tmean or CLUHII_Tmin. Similarly, the correlations between the trends of the nighttime SUHII and the CLUHII_Tmin were stronger than those between the nighttime SUHII and the CLUHII_Tmean or CLUHII_Tmax. This was primarily because the monitoring times of the daytime and nighttime SUHII were close to the monitoring times of the CLUHII_Tmax and CLUHII_Tmin, respectively.

4.3. Drivers of the trends of the CLUHII and SUHII

Human activities were the main factors causing the increase in the CLUHII and SUHII (Figs. 7–9). In approximately half of the cities, the CLUHII and SUHII were significantly and positively related to the ΔPIS, significantly and negatively related to the ΔEVI, and significantly and positively related to the ΔNL (Fig. 7). ISs have a large heat storage and low albedo. They can absorb a large amount of heat during the daytime and subsequently release it slowly during the nighttime (Imhoff et al., 2010; Zhou et al., 2014). Therefore, a larger ΔPIS was expected to have

Table 2
Number of cities with trends of significant increases in the CLUHII and SUHII.

	Spring	Summer	Autumn	Winter
Number of cities with a significant increasing trend				
CLUHI_Tmean	204	218	139	91
CLUHI_Tmax	183	156	93	71
CLUHI_Tmin	168	178	119	99
Daytime SUHII	193	245	147	64
Nighttime SUHII	154	190	153	115
Numbers of cities with a significant decreasing trend				
CLUHI_Tmean	6	1	13	22
CLUHI_Tmax	1	3	32	23
CLUHI_Tmin	17	11	22	22
Daytime SUHII	13	5	23	63
Nighttime SUHII	8	4	7	13

Table 3
Trends (°C/decade) of Ts and Ta in urban and rural areas averaged for 272 cities for the 2001–2018 period.

	Spring	Summer	Autumn	Winter
Urban areas				
Mean Ta	0.583*	0.501**	0.205	0.160
Maximum Ta	0.612	0.490**	−0.110	0.189
Minimum Ta	0.528	0.554**	0.477*	0.129
Daytime Ts	1.095**	1.367**	0.285	0.232
Nighttime Ts	0.847*	0.802**	0.620*	0.269
Rural areas				
Mean Ta	0.320	0.256	0.096	0.068
Maximum Ta	0.358	0.316	−0.180	0.131
Minimum Ta	0.298	0.364*	0.346	−0.007
Daytime Ts	0.304	0.234	−0.090	0.237
Nighttime Ts	0.493	0.420*	0.329	0.024

Significance levels:
* $p < 0.05$.
** $p < 0.01$.

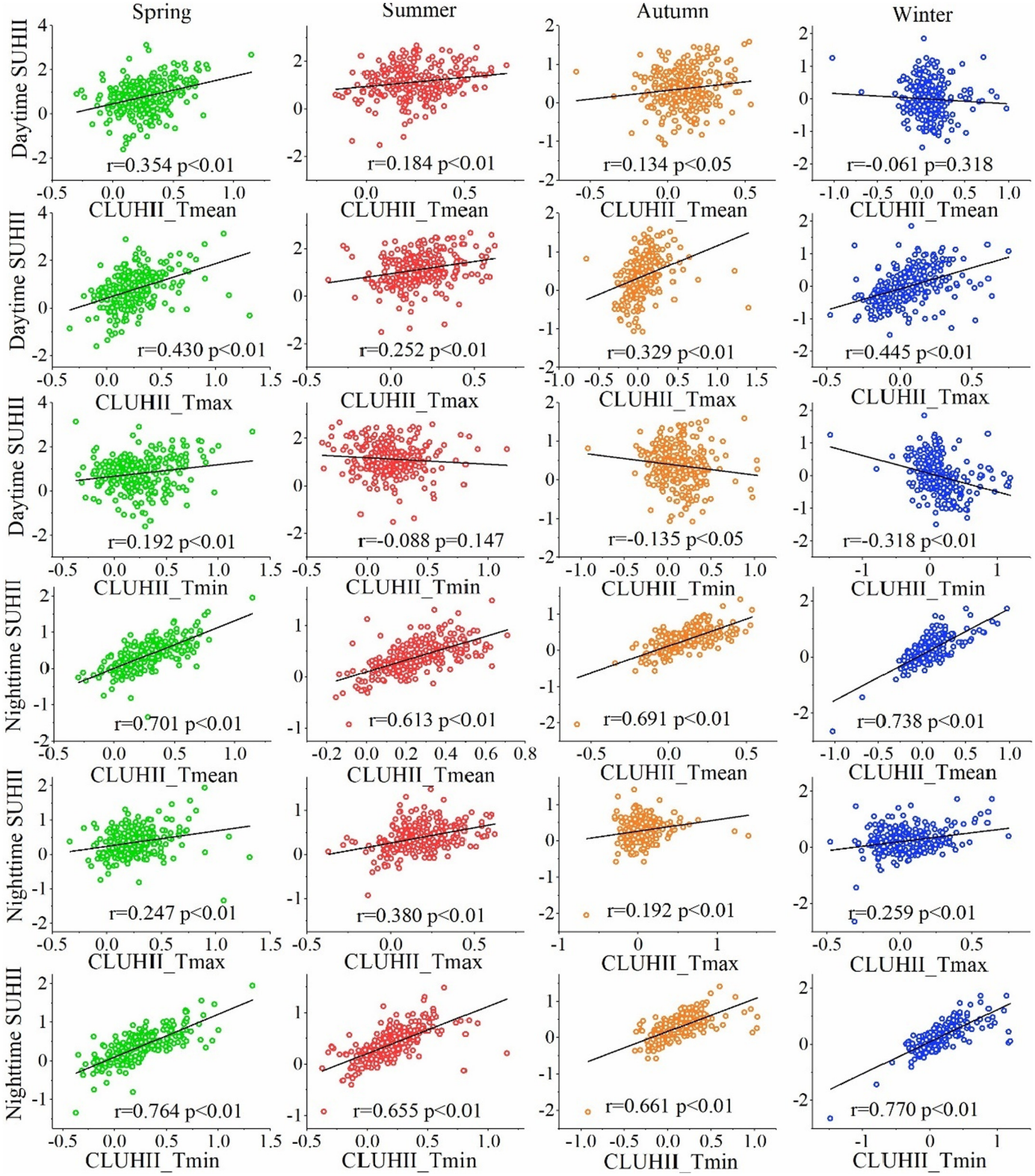

Fig. 6. Relationships between the trends of the CLUHII and SUHII (°C/decade).

a higher CLUHII and SUHII. Vegetation can decrease the temperature through evapotranspiration and lead to a shading effect. It has been widely proven to be an effective way to alleviate the UHI effect (Anniballe et al., 2014; Yao et al., 2019; Zhou et al., 2019). As a result, a large ΔEVI was generally accompanied by a lower CLUHII and SUHII. Satellite-derived NL data are an important source for monitoring human activities. They are strongly related to many human activity factors, such as the amount of ISs (Liu et al., 2012; Zhao et al., 2020) and anthropogenic heat release (Liao et al., 2017a). Therefore, the ΔNL has strong relationships with the CLUHII and SUHII.

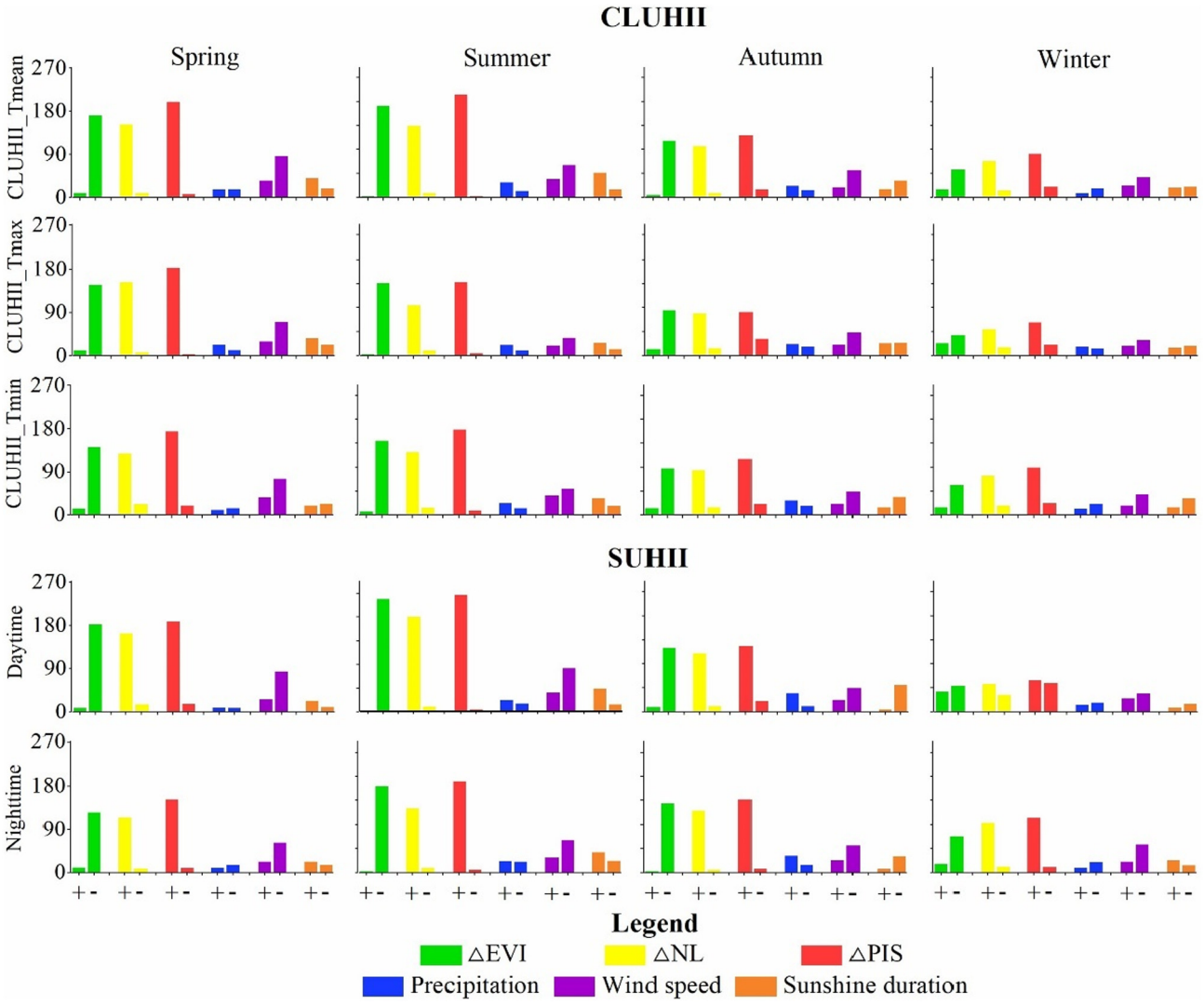

Fig. 7. Number of cities with significant correlations between the UHII and associated determinants. "+" and "−" indicate positive and negative correlations, respectively.

Among the three human activity factors, the ΔPIS was more strongly related to the UHII than the ΔEVI and ΔNL. The number of cities with significant correlations between the UHII and ΔPIS was slightly higher than that with significant correlations between the UHII and ΔEVI or ΔNL (Fig. 7). Furthermore, the number of cities with ΔPIS as the most important driver (highest absolute value of the correlation coefficient) was much greater than that with ΔEVI or ΔNL as the most important driver (Fig. 8). This occurred because ΔPIS not only represents the IS area, but also relates to vegetation coverage and anthropogenic heat release, which directly relate to the UHII. In addition, the correlation between the UHII and ΔNL was weaker than that between the UHII and ΔPIS or ΔEVI. This might be explained by the relatively low quality of the NL data. We found that the NL decreased in urban areas in some cities (e.g., Yichun, Hegang, and Qitaihe) during 2001–2018. This was not in line with the actual situation of rapid and widespread urbanization in the mainland of China (Kuang et al., 2016; Liu et al., 2014).

The meteorological factors were significantly correlated with the CLUHII and SUHII in few cities, thereby indicating that meteorological factors were not the major driving forces for most cities. This result is different from the previous studies that showed a clear control on CLUHII by meteorological factors (Yow, 2007). The possible reason is that: (1) these previous papers studied CLUHI on a short time scale, but this study analyzed the trends of seasonal mean CLUHI. The seasonal mean meteorological variables may not change significantly, and have a relatively small effect on CLUHI. (2) the mainland of China has undergone rapid urbanization during the study period. The effect of meteorological factors was masked by urbanization factors. This result is also different from a project study, which showed that the long-term climate change can affect the CLUHI (McCarthy et al., 2010). This is probably because the time period of this study (18 years) is relatively short.

Seasonally, the relationships between human activities and the UHII were stronger in spring and summer than in autumn and winter. For example, there were 171, 191, 118, and 58 cities with significant and negative correlations between the CLUHII_Tmean and the ΔEVI in spring, summer, autumn, and winter, respectively (Fig. 7). This phenomenon could be attributed to two main reasons. First, the trends of more significant decreases in the ΔEVI in spring and summer than in autumn and winter. Further analysis showed that the average decreasing rates of the ΔEVI were −0.0036/year ($p < 0.01$), −0.0048/year ($p < 0.01$), −0.0031/year ($p < 0.01$) and −0.0023/year ($p < 0.01$) in spring, summer, autumn, and winter, respectively, averaged for 272 cities. In spring and summer, trends of significant decreases in the ΔEVI could lead to an increase in the UHII, whereas the ΔEVI was relatively stable in autumn and winter. Therefore, the UHII will also be stable and affected by other factors in autumn and winter. Second, the definition of the seasons was another reason.

Diurnally, there were no significant differences between the drivers of the three types of CLUHII. For the SUHII, the ΔEVI was more strongly

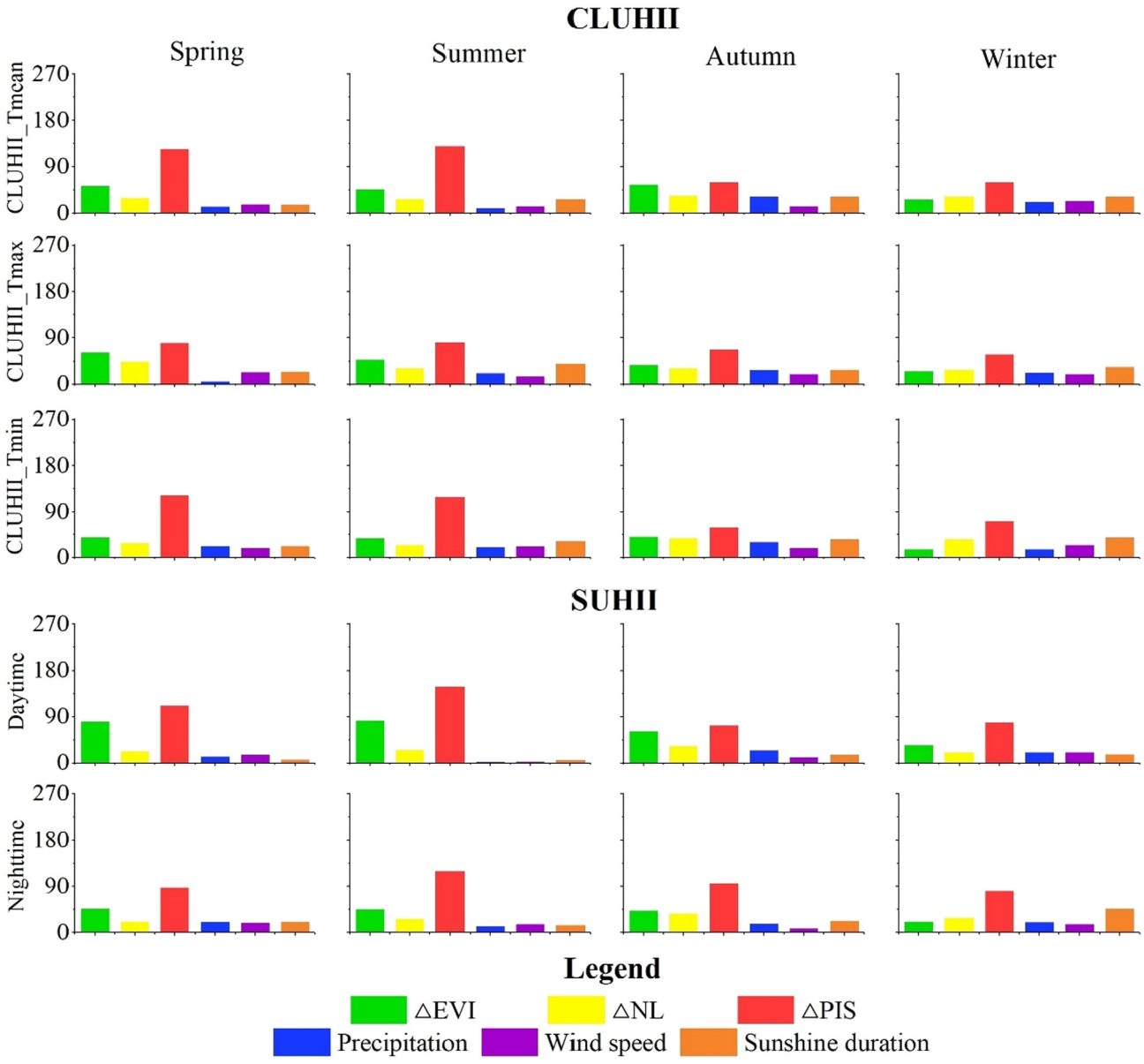

Fig. 8. Number of cities for each associated determinant with the highest absolute correlation coefficient value among all the associated determinants.

related to the daytime SUHII than to the nighttime SUHII. For example, the relative importance of the ΔEVI to the summer daytime and nighttime SUHII averaged for 272 cities was 26.3% and 20.6%, respectively (Fig. 9). This was primarily because vegetation evapotranspiration generally occurs during the daytime rather than the nighttime (Peng et al., 2012; Yao et al., 2017a). In addition, in spring and summer, the relationships between the daytime SUHII and human activity factors were stronger than those between the other types of UHII (nighttime SUHII, CLUHII_Tmean, CLUHII_Tmax, and CLUHII_Tmin) and human activity factors. This occurred because the daytime SUHII was more affected by the changes in land cover (e.g., ΔPIS) and surface characteristics (e.g., ΔEVI).

5. Discussion

5.1. Satellite-based Ta estimation

Traditionally, the Ta is monitored using station observations at a height of 2 m. The Ta data obtained using this method have a high precision and temporal resolution. However, this method has some disadvantages. The most serious problem is that the meteorological stations are sparsely distributed. Previous studies generally used one or several meteorological stations to represent the Ta of the entire urban or rural area, and then analyzed the CLUHI effect (Hu et al., 2019; Wang et al., 2015; Yang et al., 2011; Liao et al., 2017b; Ren and Zhou, 2014). This can cause great uncertainty if, for example, the urban meteorological stations are located in urban green spaces, the CLUHII will be underestimated. Similarly, when the rural meteorological stations are located in rural settlements or suburban areas, the UHII will also be underestimated. Furthermore, there are very few meteorological stations in mountains, deserts, and underdeveloped areas. Therefore, it is difficult to accurately reveal the Ta and CLUHI effect variations in these areas.

Satellite data have complete spatial coverage. Some satellite variables are strongly related to the Ta. Thus, they can be used to map Ta data. In this study, the Ta was mapped using satellite data and a matching learning algorithm. The developed Ta data had complete spatial coverage with 1 km spatial resolution, and thus could avoid the abovementioned uncertainties caused by the use of weather stations. However, compared with the station-based method, the satellite-based method has two main disadvantages. First, the time series of satellite data is relatively short.

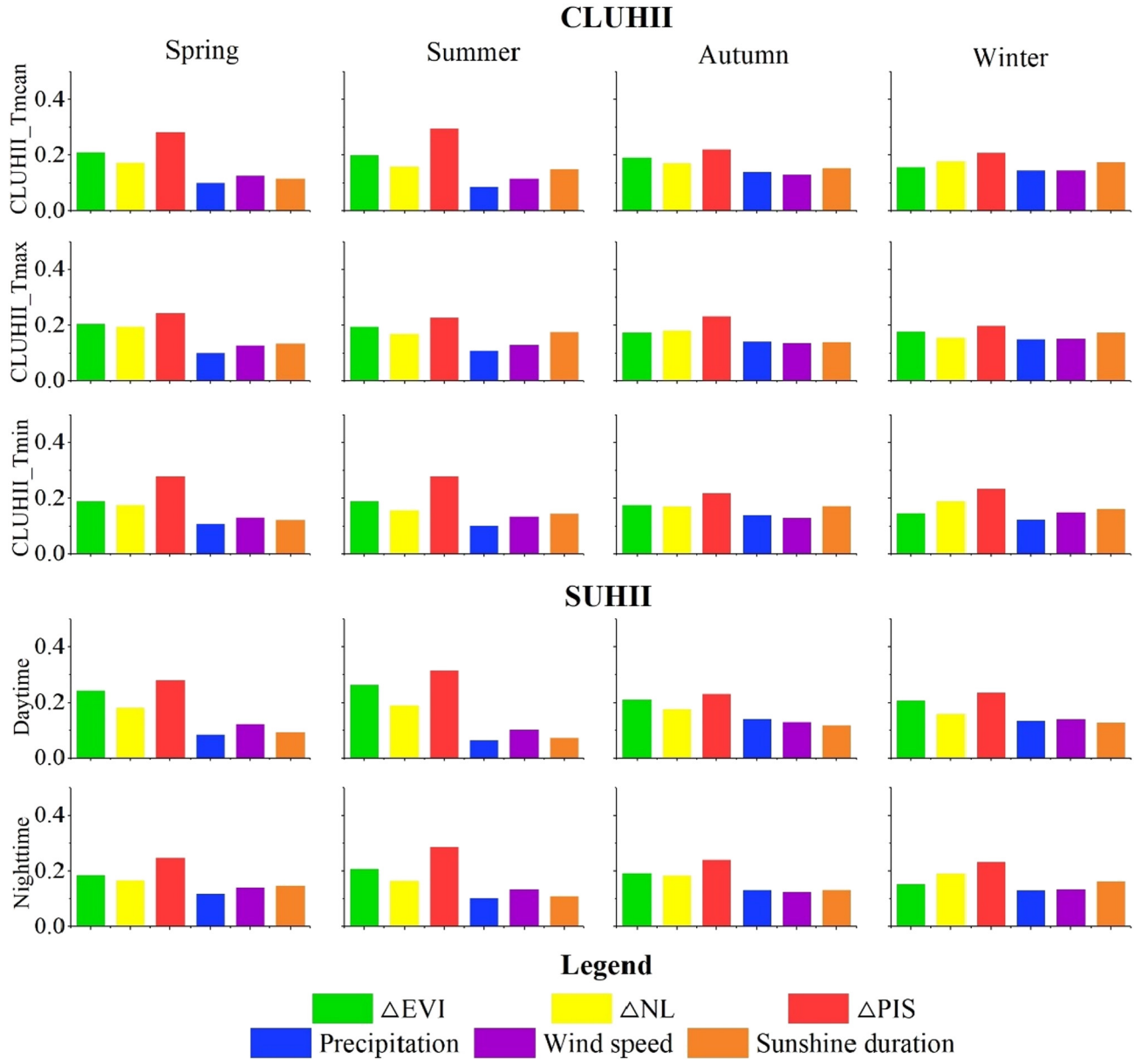

Fig. 9. Relative importance of each influencing factor averaged for 272 cities.

MODIS data have been available since February 2000. As a result, this study analyzed the UHI effect for only 18 years, which is relatively short. Second, although the accuracy of the developed Ta data in this study was higher than that in previous studies, its accuracy was still lower than that of the observed Ta data. Despite these shortcomings, the satellite-based method is promising because (1) the study period can be prolonged with the extension of the satellite data time series in the future and (2) the accuracy of the Ta can be further improved with the improvement of the satellite data quality and matching learning algorithm. It should be noted that climate model is also a promising method to investigate CLUHI, because it can: (1) provide complete spatial coverage Ta data; (2) analyze historical change of CLUHI (Oleson et al., 2010); and (3) project future trend of CLUHI (McCarthy et al., 2010).

5.2. Increased UHII

In this study, the CLUHII and SUHII increased significantly in the mainland of China during 2001–2018. This result is similar to many previous studies (Yao et al., 2017a; Yang et al., 2019; Varquez and Kanda, 2018). Urbanization is the main factor causing the increase of UHII. As urbanization will not stop, the UHII will continue to increase in the future (Zhang et al., 2020; Kim et al., 2016; Doan and Kusaka, 2018; Masson et al., 2020). The rising UHII will continuously cause negative effects on humans and the environment. First, the UHI effect can increase mortality. Goggins et al. (2012) found that a 1 °C increase in temperature leads to a 4.1% increase in mortality in areas with a high UHII. Second, the UHI effect can affect human comfort and health. Jenerette et al. (2016) found that the urban daytime Ts was strongly related to heat-related illnesses. Third, the UHI effect can increase energy consumption. A 0.45 °C increase in temperature will cause a 1.5–2.0% increase in electricity consumption in large cities (Akbari et al., 2015). Finally, the UHI effect can increase the concentrations of atmospheric pollutants (NO_2, CO_2, and CO) (Lai and Cheng, 2009). Even worse, the intensified UHI effect will overlap with the effect of global warming, further increasing the urban temperatures (Table 3). Therefore, more attention should be paid to the increase in the UHII in the mainland of

China. Some mitigation strategies should be considered, such as increasing the vegetation cover (Peng et al., 2012; Yao et al., 2017a) and utilizing reflective pavement and roofs (Akbari and Matthews, 2012; Roman et al., 2016).

5.3. Limitations

Some limitations exist in this study. First, this study validated the accuracy of the estimated Ta and showed that the accuracy of the present study was higher than that of most previous studies. However, the accuracy of the CLUHII was not validated. The verification of the accuracy of the CLUHII requires dense in situ Ta data. Most stations used in this study are located in or around urban areas. It is hard to select enough rural stations that are free from CLUHI effect to verify the accuracy of CLUHI. Denser in situ Ta data are hard to obtain. Therefore, the accuracy of the CLUHII should be verified in future works. Second, some drivers (e.g., sky view factor and thermal admittance (Oke et al., 1991)) of UHI were not analyzed in this work. This is because long time series, high spatial resolution and national coverage of these data are hard to obtain. These factors should be considered in future works.

6. Conclusions

In this study, the temporal trends of the CLUHII and SUHII and their drivers were systematically revealed in the mainland of China for the 2001–2018 period. The Cubist model produced accurate Ta estimates, with the MAE ranging from 0.289 °C to 0.455 °C. For 272 cities combined, the increasing rate of the CLUHII ranged from 0.057 °C/decade to 0.263 °C/decade ($p < 0.01$ in all cases). The SUHII also increased significantly, except for the daytime SUHII in winter. Human activities were the major driving forces of the increases in the CLUHII and SUHII. The ΔPIS was significantly correlated with the CLUHII and SUHII in approximately half of the cities, whereas meteorological factors were significantly correlated with the CLUHII and SUHII in a few cities.

Overall, this study highlights the significant trends of increases in the CLUHII and SUHII in the mainland of China. Future studies should: (1) investigate the trend of the CLUHI effect for a longer period; (2) further improve the accuracy of Ta estimation, and validate the accuracy of CLUHII; (3) analyze more drivers (e.g., sky view factor and thermal admittance) of UHI.

CRediT authorship contribution statement

Rui Yao: Data curation, Writing- Original draft preparation, revision.
Lunche Wang: Conceptualization, Methodology, Software, Reviewing and Editing, Supervision, Project administration, Funding acquisition, revision.
Xin Huang: Methodology, Software, Supervision.
Yuting Liu: Methodology, Software, revision.
Zigeng Niu: Software, Funding acquisition.
Shaoqiang Wang: Methodology, Software, revision.
Lizhe Wang: Software, Funding acquisition, revision.

Declaration of competing interest

The authors declare that they have no known competing financial interests or personal relationships that could have appeared to influence the work reported in this paper.

Acknowledgement

This work was financially supported by the National Natural Science Foundation of China (41925007, 41771360, 41975044 and 41801021), the Special Fund for Basic Scientific Research of Central Colleges, China University of Geosciences, Wuhan (CUGL170401 and CUGCJ1704), and the Fundamental Research Funds for National Universities, China University of Geosciences, Wuhan.

Appendix A

Cubist is a rule-based regression model, which originates from the M5 model tree and is an extension of the decision tree model. Cubist does not generate a final model, but produces a series of rules associated with various models. Subsequently, a series of independent variables will select a final model according to the fitting performance of the rule. Cubist is originally a commercial software, but currently can be implemented through R software and has been widely used in regression and classification applications. In this study, Cubist algorithm was performed using “Cubist” add-on package in R software. Parameters of the Cubist model were tested and determined using “caret” add-on package in R software.

References

Akbari, H., Matthews, H.D., 2012. Global cooling updates: reflective roofs and pavements. Energ. Buildings. 55, 2–6.
Akbari, H., Cartalis, C., Kolokotsa, D., Muscio, A., Pisello, A.L., Rossi, F., Santamouris, M., Synnefa, A., Wong, N.H., Zinzi, M., 2015. Local climate change and urban heat island mitigation techniques – the state of the art. J. Civ. Eng. Manag. 22, 1–16.
Anniballe, R., Bonafoni, S., Pichierri, M., 2014. Spatial and temporal trends of the surface and air heat island over Milan using MODIS data. Remote Sens. Environ 150, 163–171.
Arnfield, A.J., 2003. Two decades of urban climate research: a review of turbulence, exchanges of energy and water, and the urban heat island. Int. J. Climatol. 23, 1–26.
Danielson, J.J., Gesch, D.B., 2011. Global multi-resolution terrain elevation data 2010 (GMTED2010). U.S. Geological Survey Open-File Report 2011–1073.
Doan, V.Q., Kusaka, H., 2018. Projections of urban climate in the 2050s in a fast-growing city in Southeast Asia: the greater Ho Chi Minh City metropolitan area, Vietnam. Int. J. Climatol. 38, 4155–4171.
Dousset, B., 1989. AVHRR-derived cloudiness and surface temperature patterns over the Los Angeles area and their relationship to land use. Proceedings of IGARSS-89. IEEE, New York, NY, pp. 2132–2137.
Du, H., Wang, D., Wang, Y., Zhao, X., Qin, F., Jiang, H., Cai, Y., 2016. Influences of land cover types, meteorological conditions, anthropogenic heat and urban area on surface urban heat island in the Yangtze River Delta Urban Agglomeration. Sci. Total Environ. 571, 461–470.
Founda, D., Pierros, F., Petrakis, M., Zerefos, C., 2015. Interdecadal variations and trends of the Urban Heat Island in Athens (Greece) and its response to heat waves. Atmos. Res. 161–162, 1–13.
Goggins, W.B., Chan, E.Y., Ng, E., Ren, C., Chen, L., 2012. Effect modification of the association between short-term meteorological factors and mortality by urban heat islands in Hong Kong. PLoS One 7, e38551.
Gong, P., Li, X., Wang, J., Bai, Y., Chen, B., Hu, T., Liu, X., Xu, B., Yang, J., Zhang, W., Zhou, Y., 2020. Annual maps of global artificial impervious area (GAIA) between 1985 and 2018. Remote Sens. Environ. 236, 111510.
Grimm, N.B., Faeth, S.H., Golubiewski, N.E., Redman, C.L., Wu, J., Bai, X., Briggs, J.M., 2008. Global change and the ecology of cities. Science 319, 756–760.
Hooker, J., Duveiller, G., Cescatti, A., 2018. A global dataset of air temperature derived from satellite remote sensing and weather stations. Sci. Data 5, 180246.
Hourdin, F., Mauritsen, T., Gettelman, A., Golaz, J.C., Balaji, V., Duan, Q., Folini, D., Ji, D., Klocke, D., Qian, Y., Rauser, F., Rio, C., Tomassini, L., Watanabe, M., Williamson, D., 2017. The art and science of climate model tuning. Bull. Am. Meteorol. Soc. 98 (3), 589–602.
Hu, Y., Hou, M., Jia, G., Zhao, C., Zhen, X., Xu, Y., 2019. Comparison of surface and canopy urban heat islands within megacities of eastern China. ISPRS J. Photogramm. 156, 160–168.
Imhoff, M.L., Zhang, P., Wolfe, R.E., Bounoua, L., 2010. Remote sensing of the urban heat island effect across biomes in the continental USA. Remote Sens. Environ. 114, 504–513.
Janatian, N., Sadeghi, M., Sanaeinejad, S.H., Bakhshian, E., Farid, A., Hasheminia, S.M., Ghazanfari, S., 2017. A statistical framework for estimating air temperature using MODIS land surface temperature data. Int. J. Climatol. 37, 1181–1194.
Jenerette, G.D., Harlan, S.L., Buyantuev, A., Stefanov, W.L., Declet-Barreto, J., Ruddell, B.L., Myint, S.W., Kaplan, S., Li, X., 2016. Micro-scale urban surface temperatures are related to land-cover features and residential heat related health impacts in Phoenix, AZ USA. Landsc. Ecol. 31, 745–760.
Kim, H., Kim, Y.K., Song, S.K., Lee, H.W., 2016. Impact of future urban growth on regional climate changes in the Seoul Metropolitan Area, Korea. Sci. Total Environ. 571, 355–363.
Kloog, I., Nordio, F., Coull, B.A., Schwartz, J., 2014. Predicting spatiotemporal mean air temperature using MODIS satellite surface temperature measurements across the Northeastern USA. Remote Sens. Environ. 150, 132–139.
Kuang, W., Liu, J., Dong, J., Chi, W., Zhang, C., 2016. The rapid and massive urban and industrial land expansions in China between 1990 and 2010: a CLUD-based analysis of their trajectories, patterns, and drivers. Landscape Urban Plan 145, 21–33.

Lai, L.W., Cheng, W.L., 2009. Air quality influenced by urban heat island coupled with synoptic weather patterns. Sci. Total Environ. 407, 2724–2733.
Li, L., Zha, Y., 2019a. Estimating monthly average temperature by remote sensing in China. Adv. Space Res. 63, 2345–2357.
Li, L., Zha, Y., 2019b. Satellite-based spatiotemporal trends of canopy urban heat islands and associated drivers in China's 32 major cities. Remote Sens. 11, 102.
Li, X., Zhou, Y., Asrar, G.R., Imhoff, M., Li, X., 2017. The surface urban heat island response to urban expansion: a panel analysis for the conterminous United States. Sci. Total Environ. 605–606, 426–435.
Li, X., Zhou, Y., Asrar, G.R., Zhu, Z., 2018. Developing a 1 km resolution daily air temperature dataset for urban and surrounding areas in the conterminous United States. Remote Sens. Environ. 215, 74–84.
Li, H., Zhou, Y., Wang, X., Zhou, X., Zhang, H., Sodoudi, S., 2019. Quantifying urban heat island intensity and its physical mechanism using WRF/UCM. Sci. Total Environ. 650, 3110–3119.
Li, X., Zhou, Y., Zhao, M., Zhao, X., 2020. A harmonized global nighttime light dataset 1992–2018. Sci Data 7, 168.
Liao, W., Liu, X., Wang, D., Sheng, Y., 2017a. The impact of energy consumption on the surface urban heat island in China's 32 major cities. Remote Sens. 9, 250.
Liao, W., Wang, D., Liu, X., Wang, G., Zhang, J., 2017b. Estimated influence of urbanization on surface warming in Eastern China using time-varying land use data. Int. J. Climatol. 37, 3197–3208.
Liu, Z., He, C., Zhang, Q., Huang, Q., Yang, Y., 2012. Extracting the dynamics of urban expansion in China using DMSP-OLS nighttime light data from 1992 to 2008. Landscape Urban Plan 106, 62–72.
Liu, J., Kuang, W., Zhang, Z., Xu, X., Qin, Y., Ning, J., Zhou, W., Zhang, S., Li, R., Yan, C., Wu, S., Shi, X., Jiang, N., Yu, D., Pan, X., Chi, W., 2014. Spatiotemporal characteristics, patterns, and causes of land-use changes in China since the late 1980s. J. Geogr. Sci. 24, 195–210.
Liu, K., Li, X., Wang, S., Li, Y., 2020. Investigating the impacts of driving factors on urban heat islands in southern China from 2003 to 2015. J. Clean. Prod. 254, 120141.
Lu, N., Liang, S., Huang, G., Qin, J., Yao, L., Wang, D., Yang, K., 2018. Hierarchical Bayesian space-time estimation of monthly maximum and minimum surface air temperature. Remote Sens. Environ. 211, 48–58.
Mac, N.R., 2000. Regression and model-building in conservation biology, biogeography and ecology: the distinction between - and reconciliation of – 'predictive' and 'explanatory' models. Biodivers. Conserv. 9, 655–671.
Marthews, T.R., Dadson, S.J., Lehner, B., Abele, S., Gedney, N., 2015. High-resolution global topographic index values for use in large-scale hydrological modelling. Hydrol. Earth Syst. Sc. 19, 91–104.
Masson, V., Lemonsu, A., Hidalgo, J., Voogt, J., 2020. Urban climates and climate change. Annu. Rev. Environ. Resour. 45, 411–444.
McCarthy, M.P., Best, M.J., Betts, R.A., 2010. Climate change in cities due to global warming and urban effects. Geophys. Res. Lett. 37, L09705.
Mertes, C.M., Schneider, A., Sulla-Menashe, D., Tatem, A.J., Tan, B., 2015. Detecting change in urban areas at continental scales with MODIS data. Remote Sens. Environ. 158, 331–347.
Meyer, H., Katurji, M., Appelhans, T., Müller, M., Nauss, T., Roudier, P., Zawar-Reza, P., 2016. Mapping daily air temperature for Antarctica based on MODIS LST. Remote Sens. 8, 732.
Noi, P., Degener, J., Kappas, M., 2017. Comparison of multiple linear regression, cubist regression, and random forest algorithms to estimate daily air surface temperature from dynamic combinations of MODIS LST data. Remote Sens. 9, 398.
Oke, T.R., 1981. Canyon geometry and the nocturnal heat island: comparison of scale model and field observations. J. Climatol. 1, 237–254.
Oke, T.R., Johnson, G.T., Steyn, D.G., Watson, I.D., 1991. Simulation of surface urban heat islands under 'ideal' conditions at night. Part 2: diagnosis of causation. Bound.-Layer Meteorol. 56, 339–358.
Oleson, K.W., Bonan, G.B., Feddema, J., 2010. Effects of white roofs on urban temperature in a global climate model. Geophys. Res. Lett. 37, L03701.
Park, B.J., Kim, Y.H., Min, S.K., Kim, M.K., Choi, Y., Boo, K.O., Shim, S., 2017. Long-term warming trends in Korea and contribution of urbanization: an updated assessment. J. Geophys. Res.-Atmos. 122, 10,637–10,654.
Patz, J.A., Campbell-Lendrum, D., Holloway, T., Foley, J.A., 2005. Impact of regional climate change on human health. Nature 438, 310–317.
Peng, S., Piao, S., Ciais, P., Friedlingstein, P., Ottle, C., Breon, F.M., Nan, H., Zhou, L., Myneni, R.B., 2012. Surface urban heat island across 419 global big cities. Environ. Sci. Technol. 46, 696–703.
Peng, J., Jia, J., Liu, Y., Li, H., Wu, J., 2018. Seasonal contrast of the dominant factors for spatial distribution of land surface temperature in urban areas. Remote Sens. Environ. 215, 255–267.
Pichierri, M., Bonafoni, S., Biondi, R., 2012. Satellite air temperature estimation for monitoring the canopy layer heat island of Milan. Remote Sens. Environ. 127, 130–138.
Quinlan, R., 1992. Learning with continuous classes. Proceedings of the 5th Australia Joint Conference on Artificial Intelligence, Hobart, Tasmania, pp. 343–348.
Ren, G., Zhou, Y., 2014. Urbanization effect on trends of extreme temperature indices of national stations over mainland China, 1961–2008. J. Clim. 27, 2340–2360.
Ren, G., Zhou, Y., Chu, Z., Zhou, J., Zhang, A., Guo, J., Liu, X., 2008. Urbanization effects on observed surface air temperature trends in North China. J. Clim. 21, 1333–1348.
Roman, K.K., O'Brien, T., Alvey, J.B., Woo, O., 2016. Simulating the effects of cool roof and PCM (phase change materials) based roof to mitigate UHI (urban heat island) in prominent US cities. Energy 96, 103–117.
Santamouris, M., Papanikolaou, N., Livada, I., Koronakis, I., Georgakis, C., Argiriou, A., Assimakopoulos, D.N., 2001. On the impact of urban climate on the energy consumption of buildings. Sol. Energy 70, 201–216.
Shen, H., Jiang, Y., Li, T., Cheng, Q., Zeng, C., Zhang, L., 2020. Deep learning-based air temperature mapping by fusing remote sensing, station, simulation and socioeconomic data. Remote Sens. Environ. 240, 111692.
United Nations, 2018. World Urbanization Prospects: The 2018 Revision.
Vancutsem, C., Ceccato, P., Dinku, T., Connor, S.J., 2010. Evaluation of MODIS land surface temperature data to estimate air temperature in different ecosystems over Africa. Remote Sens. Environ. 114, 449–465.
Varquez, A.C.G., Kanda, M., 2018. Global urban climatology: a meta-analysis of air temperature trends (1960–2009). NPJ Clim. Atmos. Sci. 1, 32.
Voogt, J.A., Oke, T.R., 2003. Thermal remote sensing of urban climates. Remote Sens. Environ. 86, 370–384.
Wang, F., Ge, Q., Wang, S., Li, Q., Jones, P.D., 2015. A new estimation of urbanization's contribution to the warming trend in China. J. Clim. 28, 8923–8938.
Xu, Y., Knudby, A., Shen, Y., Liu, Y., 2018. Mapping monthly air temperature in the Tibetan Plateau from MODIS data based on machine learning methods. IEEE J-STARS 11, 345–354.
Yang, X., Hou, Y., Chen, B., 2011. Observed surface warming induced by urbanization in east China. J. Geophys. Res. 116, D14113.
Yang, Q., Huang, X., Tang, Q., 2019. The footprint of urban heat island effect in 302 Chinese cities: temporal trends and associated factors. Sci. Total Environ. 655, 652–662.
Yao, R., Wang, L., Huang, X., Niu, Z., Liu, F., Wang, Q., 2017a. Temporal trends of surface urban heat islands and associated determinants in major Chinese cities. Sci. Total Environ. 609, 742–754.
Yao, R., Wang, L., Gui, X., Zheng, Y., Zhang, H., Huang, X., 2017b. Urbanization effects on vegetation and surface urban heat islands in China's Yangtze River Basin. Remote Sens. 9, 540.
Yao, R., Wang, L., Huang, X., Niu, Y., Chen, Y., Niu, Z., 2018a. The influence of different data and method on estimating the surface urban heat island intensity. Ecol. Indic. 89, 45–55.
Yao, R., Wang, L., Huang, X., Zhang, W., Li, J., Niu, Z., 2018b. Interannual variations in surface urban heat island intensity and associated drivers in China. J. Environ. Manag. 222, 86–94.
Yao, R., Wang, L., Huang, X., Gong, W., Xia, X., 2019. Greening in rural areas increases the surface urban heat island intensity. Geophys. Res. Lett. 46, 2204–2212.
Yao, R., Wang, L., Huang, X., Li, L., Sun, J., Wu, X., Jiang, W., 2020. Developing a temporally accurate air temperature dataset for Mainland China. Sci. Total Environ. 706, 136037.
Yoo, C., Im, J., Park, Quackenbush, L.J., 2018. Estimation of daily maximum and minimum air temperatures in urban landscapes using MODIS time series satellite data. ISPRS J. Photogramm. 137, 149–162.
Yow, D.M., 2007. Urban heat islands: observations, impacts and adaptations. Geogr. Compass 1, 1227–1251.
Zhan, W., Ju, W., Hai, S., Ferguson, G., Quan, J., Tang, C., Guo, Z., Kong, F., 2014. Satellite-derived subsurface urban heat island. Environ. Sci. Technol. 48, 12134–12140.
Zhang, H., Zhang, F., Ye, M., Che, T., Zhang, G., 2016. Estimating daily air temperatures over the Tibetan Plateau by dynamically integrating MODIS LST data. J. Geophys. Res.-Atmos. 121, 11425–11441.
Zhang, D., Wang, X., Qu, L., Li, S., Lin, Y., Yao, R., Zhou, X., Li, J., 2020. Land use/cover predictions incorporating ecological security for the Yangtze River Delta region, China. Ecol. Indic. 119, 106841.
Zhao, M., Zhou, Y., Li, X., Cheng, W., Zhou, C., Ma, T., Li, M., Huang, K., 2020. Mapping urban dynamics (1992–2018) in Southeast Asia using consistent nighttime light data from DMSP and VIIRS. Remote Sens. Environ. 248, 111980.
Zhou, D., Zhao, S., Liu, S., Zhang, L., Zhu, C., 2014. Surface urban heat island in China's 32 major cities: spatial patterns and drivers. Remote Sens. Environ. 152, 51–61.
Zhou, D., Zhang, L., Li, D., Huang, D., Zhu, C., 2016. Climate–vegetation control on the diurnal and seasonal variations of surface urban heat islands in China. Environ. Res. Lett. 11, 074009.
Zhou, D., Xiao, J., Bonafoni, S., Berger, C., Deilami, K., Zhou, Y., Frolking, S., Yao, R., Qiao, Z., Sobrino, J., 2019. Satellite remote sensing of surface urban heat islands: progress, challenges, and perspectives. Remote Sens. 11, 48.
Zhou, B., Erell, E., Hough, I., Rosenblatt, J., Just, A.C., Novack, V., Kloog, I., 2020. Estimating near-surface air temperature across Israel using a machine learning based hybrid approach. Int. J. Climatol. https://doi.org/10.3390/rs11010048.
Zhu, W., Lű, A., Jia, S., Yan, J., Mahmood, R., 2017. Retrievals of all-weather daytime air temperature from MODIS products. Remote Sens. Environ. 189, 152–163.